

---

# BEYOND SINGLE-GPU: SCALING PDLP TO DISTRIBUTED MULTI-GPU SYSTEMS

---

Hongpei Li<sup>1</sup>, Yicheng Huang<sup>2</sup>, Huihang Liu<sup>3</sup>, Dongdong Ge<sup>3</sup>, Yinyu Ye<sup>4</sup>

<sup>1</sup> Cardinal Operations

<sup>2</sup> Shanghai University of Finance and Economics

<sup>3</sup> Shanghai Jiao Tong University

<sup>4</sup> Stanford University

ishongpeili@gmail.com, hk11u@sjtu.edu.cn, ddge@sjtu.edu.cn

## ABSTRACT

In this work, we present a distributed implementation of the Primal-Dual Hybrid Gradient (PDHG) algorithm for solving massive-scale linear programming (LP) problems. Although PDHG-based solvers have shown strong performance on single-node GPU architectures, their applicability to industrial-scale instances is often limited by GPU memory capacity and computational throughput. To overcome these challenges, we extend the PDHG framework to a distributed-memory setting via a practical two-dimensional grid partitioning of the constraint matrix, enabling scalable execution across multiple GPUs. To improve load balance and computational efficiency, we introduce a block-wise random shuffling strategy combined with nonzero-aware data distribution. By distributing both memory and computation, the proposed framework not only overcomes the single-GPU memory bottleneck but also achieves substantial speedups by exploiting multi-GPU parallelism with relatively low communication overhead. Extensive experiments on standard LP benchmarks, including MIPLIB and Hans' instances, as well as large-scale real-world datasets, show that our distributed implementation, built upon cuPDLPx [Lu et al., 2025], achieves strong scalability and high performance while preserving full FP64 numerical accuracy.

## 1 Introduction

Large-scale linear programming (LP) lies at the core of numerous machine learning [Agarwal et al., 2018, Ben-Tal et al., 2013, Taskar et al., 2005, Joachims et al., 2009], operations research [Waissi, 1994, Gallego and Van Ryzin, 1997, Talluri and Van Ryzin, 2006], and data-driven decision-making problems, including resource allocation [Hibiki, 2006, Kelly et al., 1998], market equilibrium computation Eisenberg and Gale [1959], Orlin [2010], and multi-stage stochastic programming [Hibiki, 2006, Gangammanavar and Sen, 2021]. Modern applications often involve millions or even billions of variables and constraints, rendering classical interior-point methods impractical due to their unfavorable memory footprint and limited parallel scalability.

First-order primal-dual methods, such as PDLP [Applegate et al., 2021], cuPDLP.jl [Lu and Yang, 2023a], cuPDLP-C [Lu et al., 2023], cuPDLPx [Lu et al., 2025], and HPR-LP [Chen et al., 2025] have recently emerged as a promising alternative for solving large-scale LPs, owing to their low per-iteration complexity and amenability to parallelization. Among them, the PDLP family based on the primal-dual hybrid gradient (PDHG) framework has demonstrated strong empirical performance and robustness across a wide range of benchmark instances.

However, most existing PDLP implementations are designed for single-node or tightly coupled shared-memory environments, which limits their applicability to truly large-scale and distributed settings. As a result, their applicability to truly large-scale LP problems in distributed-memory and multi-GPU environments remains limited.

In this paper, we propose a distributed PDLP framework for solving large-scale linear programming on multi-node architectures. The proposed approach decomposes primal-dual updates across workers while coordinating global coupling constraints through lightweight communication primitives. By exploiting the intrinsic separability of PDLP updates and supporting partially synchronous execution, our framework enables scalable performance with respect to both problem size and available computational resources.

Our main contributions are summarized as follows:

- We first propose a distributed PDHG-based solver for large-scale LPs that scales across multiple GPUs.
- We introduce a block-wise random shuffling and a nonzero-aware partitioning scheme to maintain load balance under irregular sparsity.
- Extensive experiments demonstrate that the proposed approach achieves strong multi-GPU scalability and high performance on large-scale LP benchmarks, while maintaining full FP64 numerical accuracy.

While this work concentrates on LPs, the proposed distributed framework naturally generalizes to a broader class of convex optimization problems, such as quadratic programming (QP), semidefinite programming (SDP), and general conic LPs.

### 1.1 Related Works

Traditional linear programming solvers, including the simplex method and interior-point methods (IPMs), are highly effective for small- to medium-scale problems. These methods deliver reliable, high-accuracy solutions across various applications and are supported by commercial solvers such as MOSEK [ApS, 2019], GUROBI [Gurobi Optimization, 2021], and COPT [Ge et al., 2022]. However, their applicability to large-scale instances is limited: the simplex method suffers from exponential worst-case complexity, while IPMs rely on sequential matrix factorizations that are difficult to scale and parallelize. As a result, first-order methods (FOMs) have emerged as a compelling alternative for solving large-scale LPs.

Among FOM-based approaches, ADMM-based solvers such as ABIP [Lin et al., 2021] and ABIP+ [Deng et al., 2022] demonstrate the potential of first-order methods for large-scale LPs by requiring only a one-time matrix factorization. Building on this progress, PDHG-based solvers, most notably PDLP [Applegate et al., 2021] and its GPU implementation cuPDLP.jl [Lu and Yang, 2023a], eliminate the need for matrix factorization altogether and represent the first methods capable of efficiently solving truly large-scale LPs. To further scale to problem sizes that exceed the memory capacity of a single GPU, the C/CUDA-based implementation cuPDLP-C [Lu et al., 2023] was introduced. More recently, cuPDLPx [Lu et al., 2025] incorporates additional algorithmic heuristics and engineering optimizations to further improve convergence behavior and computational efficiency.

Beyond GPU-based first-order primal–dual methods developed specifically for LPs, a growing body of work has proposed GPU-accelerated solvers for a wide range of large-scale convex optimization problems. For quadratic programming, representative methods include rAPDHG [Lu and Yang, 2023b], PDHCG [Huang et al., 2024], and HPR-QP [Chen et al., 2025]. For semidefinite programming, notable GPU-based solvers include LoRADS [Han et al., 2024a,b], ALORA [Ding et al., 2025], and cuHALLaR [Aguirre et al., 2025]. More generally, PDCS [Lin et al., 2025] addresses large-scale conic programming problems. GPU-enabled primal–dual methods have also been successfully applied to optimal transport [Lu and Yang, 2024a, Zhang et al., 2025], market equilibrium computation [Liu et al., 2025], and large-scale network flow problems [Zhang and Boyd, 2025]. Collectively, these GPU-accelerated primal–dual solvers demonstrate substantial advantages over traditional approaches, particularly in terms of scalability and computational efficiency on modern parallel hardware.

## 2 Preliminaries

In this section, we briefly review the general formulation of linear programming in Section 2.1, the Primal–Dual Hybrid Gradient (PDHG) algorithm in Section 2.2, and the cuPDLPx solver [Lu et al., 2025], which serves as the foundation for our implementation, in Section 2.3.

### 2.1 Linear Programming

We consider the following linear programming problem

$$\min_{x \in \mathcal{X}} c^\top x \quad \text{subject to } Ax \in \mathcal{S} \quad (1)$$

where  $A \in \mathbb{R}^{m \times n}$ ,  $c \in \mathbb{R}^n$ , the feasible set  $\mathcal{X} := \{x \in \mathbb{R}^n : \ell_v \leq x \leq u_v\}$  with bounds  $\ell_v \in (\mathbb{R} \cup \{-\infty\})^n$  and  $u_v \in (\mathbb{R} \cup \{\infty\})^n$ , and the constraint range  $\mathcal{S} := \{s \in \mathbb{R}^m : \ell_c \leq s \leq u_c\}$  with  $\ell_c \in (\mathbb{R} \cup \{-\infty\})^m$  and  $u_c \in (\mathbb{R} \cup \{\infty\})^m$ . One can readily derive the corresponding Lagrangian, which leads to an equivalent saddle-point formulation of the form

$$\min_{x \in \mathcal{X}} \max_{y \in \mathcal{Y}} \mathcal{L}(x, y) := c^\top x + y^\top Ax - p(-y; \ell_c, u_c). \quad (2)$$

where  $p(y; \ell, u)$  is a piecewise linear function w.r.t.  $y$  defined as

$$p(y; \ell, u) = u^\top y^+ - \ell^\top y^-$$

with  $y^+ = \max\{y, 0\}$  and  $y^- = \max\{-y, 0\}$  being the positive and negative parts of  $y$ , respectively, and the dual feasible set  $\mathcal{Y} \subseteq \mathbb{R}^m$  is Cartesian product whose  $i$ -th components are determined by the boundedness of the primal

constraints:

$$\mathcal{Y}_i := \begin{cases} \{0\} & \text{if } (\ell_c)_i = -\infty, (u_c)_i = \infty, \\ \mathbb{R}^- & \text{if } (\ell_c)_i = -\infty, (u_c)_i \in \mathbb{R}, \\ \mathbb{R}^+ & \text{if } (\ell_c)_i \in \mathbb{R}, (u_c)_i = \infty, \\ \mathbb{R} & \text{otherwise.} \end{cases}$$

## 2.2 The PDHG Algorithm

The primal–dual hybrid gradient (PDHG) method can be applied to the saddle-point problem in (2), yielding the following update rules:

$$\begin{aligned} x^{k+1} &= \text{proj}_{\mathcal{X}}(x^k - \tau(c - A^\top y^k)) \\ z^{k+1} &= A(2x^{k+1} - x^k) \\ y^{k+1} &= y^k - \sigma z^{k+1} - \sigma \cdot \text{proj}_{-\mathcal{S}}(\sigma^{-1}y^k - z^{k+1}) \end{aligned} \quad (3)$$

where  $\tau$  and  $\sigma$  denote the primal and dual step sizes, respectively. The step sizes can be reparameterized as  $\tau = \frac{\eta}{\omega}$  and  $\sigma = \eta\omega$ , where  $\eta$  denotes the overall step size and  $\omega$  balances the primal and dual updates.

## 2.3 Algorithmic Enhancements in cuPDLPx

Our distributed implementation builds upon the state-of-the-art GPU-based LP solver cuPDLPx [Lu et al., 2025]. To improve convergence behavior and numerical stability, cuPDLPx incorporates several algorithmic enhancements, including

- Reflected Halpern iteration scheme;
- Adaptive restarting strategy;
- Primal weight updates.

These techniques further enhance the performance of PDLP. Detailed descriptions of these methods are provided in Appendix A.

## 2.4 Termination Criteria

The dual form of the problem is given by

$$\max_{y \in \mathcal{Y}, s \in \mathcal{R}} -p(-y; \ell_c, u_c) - p(-r; \ell_v, u_v) \quad \text{subject to } c - A^\top y = r, \quad (4)$$

where  $\mathcal{R} \subseteq \mathbb{R}^n$  is the Cartesian product whose  $i$ -th components are determined by the boundedness of the primal constraints:

$$\mathcal{R}_i := \begin{cases} \{0\} & \text{if } (\ell_v)_i = -\infty, (u_v)_i = \infty, \\ \mathbb{R}^- & \text{if } (\ell_v)_i = -\infty, (u_v)_i \in \mathbb{R}, \\ \mathbb{R}^+ & \text{if } (\ell_v)_i \in \mathbb{R}, (u_v)_i = \infty, \\ \mathbb{R} & \text{otherwise.} \end{cases} \quad (5)$$

The solver terminates when the iterates satisfy a specified tolerance  $\epsilon$  across three relative KKT error metrics: primal residual ( $r_{\text{primal}}$ ), dual residual ( $r_{\text{dual}}$ ), and the duality gap ( $r_{\text{gap}}$ ).

$$r_{\text{primal}} = \frac{\|Ax - \text{proj}_{\mathcal{S}}(Ax)\|_2}{1 + \|\ell_c, u_c\|_2}, \quad (6)$$

$$r_{\text{dual}} = \frac{\|\text{proj}_{\mathcal{X}}(x - \tau(c - A^\top y)) - x\|_2 / \tau}{1 + \|c\|_2}, \quad (7)$$

$$r_{\text{gap}} = \frac{|c^\top x + p(-y; \ell_c, u_c) - s^\top x|}{1 + \max\{|c^\top x|, |p(-y; \ell_c, u_c) + s^\top x|\}}. \quad (8)$$

where  $s = (\text{proj}_{\mathcal{X}}(x - \tau(c - A^\top y)) - (x - \tau(c - A^\top y))) / \tau$ . The overall residual is defined as  $\max\{r_{\text{primal}}, r_{\text{dual}}, r_{\text{gap}}\}$ .

## 3 Distributed PDLP

To scale PDHG beyond the memory limits of a single device, we adopt a 2D partitioning strategy for the constraint matrix  $A$ . This design enables flexible distribution of variables and constraints across a multi-GPU cluster, allowing the solver to handle problem instances that exceed the memory capacity of any individual device.

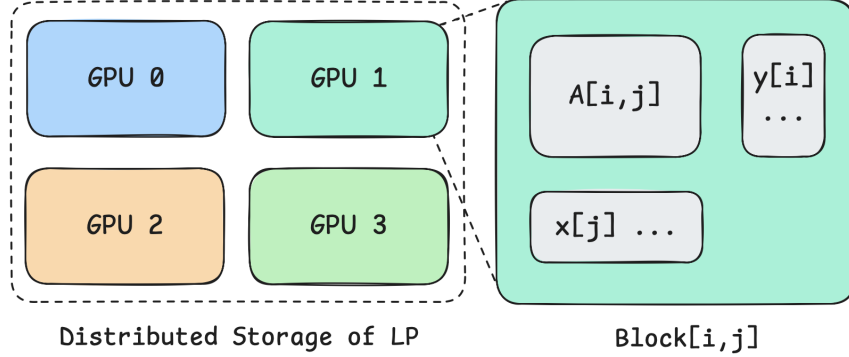


Figure 1: Distributed memory layout under 2D grid partitioning. **Left:** A logical  $2 \times 2$  device mesh illustrating the global topology. **Right:** Local data stored on the device at grid coordinate  $(i, j)$ . The constraint matrix is stored as block  $A_{[i,j]}$ , primal variables  $x_{[j]}$ , and dual variables  $y_{[i]}$ . This layout enables local computation of  $A_{[i,j]}x_{[j]}$  and  $A_{[i,j]}^\top y_{[i]}$  prior to reduction.

### 3.1 Problem Partition

We adopt a variant of the named-axis notation to describe the data layout across hardware resources [Austin et al., 2025]. Specifically, we assume a 2D grid of devices, where each axis is assigned a semantic role:

- **Row axis ( $R$ ):** Corresponds to partitioning along the rows of  $A$ , with cardinality  $|R|$ .
- **Column axis ( $C$ ):** Corresponds to partitioning along the columns of  $A$ , with cardinality  $|C|$ .

A partition  $\mathcal{P}$  is defined by mapping the dimensions of a tensor to the corresponding physical grid axes. For the sparse constraint matrix  $A \in \mathbb{R}^{m \times n}$ , applying the partition  $\mathcal{P}$  implies that the global row index set is divided into  $|R|$  disjoint subsets along the grid axis  $R$ , while the global column index set is divided into  $|C|$  disjoint subsets along the grid axis  $C$ . As a result, the matrix  $A$  is decomposed into a two-dimensional grid of local sparse blocks:

$$A \rightarrow \begin{bmatrix} A_{[1,1]} & A_{[1,2]} & \dots & A_{[1,|C|]} \\ A_{[2,1]} & A_{[2,2]} & \dots & A_{[2,|C|]} \\ \vdots & \vdots & \ddots & \vdots \\ A_{[|R|,1]} & A_{[|R|,2]} & \dots & A_{[|R|,|C|]} \end{bmatrix} \quad (9)$$

where each sub-matrix  $A_{[i,j]}$  contains the block of non-zero entries corresponding to the  $i$ -th row partition and the  $j$ -th column partition. Under this layout, each block  $A_{[i,j]}$  is stored exclusively in the local memory of the device located at grid coordinate  $(i, j)$ .

**Local Shapes and Sparsity.** In dense tensor settings, a partition  $\mathcal{P}$  typically assigns each device a uniform block of size  $(m/|R|, n/|C|)$  [Austin et al., 2025]. In contrast, our setting allows for irregular local shapes. Specifically, each device  $(i, j)$  in the grid stores a submatrix  $A_{[i,j]}$  of size  $(m_i, n_j)$ , where  $\sum_i m_i = m$  and  $\sum_j n_j = n$ . Moreover, the number of nonzero entries (NNZ) may vary significantly across devices. This irregularity motivates the load-balancing heuristics introduced in Section 3.3.

**Vector Partitioning and Replication.** To minimize communication during local computations, we align the distribution of all vectors with the two-dimensional partitioning of the constraint matrix. Primal-space vectors in  $\mathbb{R}^n$ , including the decision variable  $x$  and objective coefficients  $c$ , are partitioned along the column axis  $C$ . The  $j$ -th block, denoted by  $x_{[j]}, c_{[j]} \in \mathbb{R}^{n_j}$ , induces a local primal feasible set

$$\mathcal{X}_{[j]} := \{z \in \mathbb{R}^{n_j} : (\ell_v)_{[j]} \leq z \leq (u_v)_{[j]}\}.$$

Each block is vertically replicated across all devices in column  $j$ , ensuring that any device holding  $A_{[i,j]}$  can compute  $A_{[i,j]}x_{[j]}$  and  $\text{proj}_{\mathcal{X}_{[j]}}$  without communication.

Similarly, dual-space vectors in  $\mathbb{R}^m$ , including the dual variable  $y$ , are partitioned along the row axis  $R$ , with blocks  $y_{[i]} \in \mathbb{R}^{m_i}$  and corresponding local constraint sets

$$\mathcal{S}_{[i]} := \{b \in \mathbb{R}^{m_i} : (\ell_c)_{[i]} \leq b \leq (u_c)_{[i]}\}.$$

**Algorithm 1** Distributed Grid-Partitioned PDLP

---

**Input:** Problem instance  $(A, b, c)$ , device count  $N_{procs} \geq 2$ , permutation  $\Pi$ , partition  $\mathcal{P}$ , initial point  $(x^0, y^0)$ , step sizes  $\tau, \sigma$ , and accuracy  $\epsilon$ .

**Initialization:** Determine grid topology  $|R| \times |C| \leq N_{procs}$ . Apply permutation  $\Pi$  and partition  $\mathcal{P}$  to get

$$A \rightarrow \{A_{[i,j]}\}, b \rightarrow \{b_{[i]}\}, c \rightarrow \{c_{[j]}\}, y^0 \rightarrow \{y_{[i]}^0\}, x^0 \rightarrow \{x_{[j]}^0\}.$$

Store local blocks  $(A_{[i,j]}, b_{[i]}, c_{[j]}, x_{[j]}^0, y_{[i]}^0)$  in each  $(i, j)$ -th GPU.

**for**  $k = 0, 1, \dots$ , on each  $(i, j)$ -th GPU **do**

**1. Distributed Primal Update**

Compute local partial gradient:  $g_{[i,j]} = A_{[i,j]}^\top y_{[i]}^k$

Communication: Aggregate  $g_{[i,j]}$  across row axis  $R$  (vertical sum):  $[A^\top y^k]_{[j]} = \text{AllReduce}_R(g_{[i,j]})$

Update local primal variable:  $x_{[j]}^{k+1} = \text{proj}_{\mathcal{X}_{[j]}}(x_{[j]}^k - \tau(c_{[j]} - [A^\top y^k]_{[j]}))$

**2. Distributed Dual Update**

Compute local partial constraint:  $v_{[i,j]} = A_{[i,j]}(2x_{[j]}^{k+1} - x_{[j]}^k)$

Communication: Aggregate  $v_{[i,j]}$  across column axis  $C$  (horizontal sum):  $z_{[i]} = \text{AllReduce}_C(v_{[i,j]})$

Update local dual variable:  $y_{[i]}^{k+1} = y_{[i]}^k - \sigma z_{[i]} - \sigma \cdot \text{proj}_{-\mathcal{S}_{[i]}}(\sigma^{-1}y_{[i]}^k - z_{[i]})$

**3. Termination criterion:** Stop if the KKT error is less than  $\epsilon$ .

**end for**

---

These blocks are horizontally replicated across all devices in row  $i$ , enabling local computation of  $A_{[i,j]}^\top y_{[i]}$  and dual projections  $\text{proj}_{-\mathcal{S}_{[i]}}$ . By orthogonally replicating primal and dual variables, communication is limited to reductions of partial matrix–vector products, maximizing the efficiency of local update kernels.

### 3.2 Distributed PDHG Algorithm

The iterative updates require global synchronization of partial matrix–vector products. We perform this synchronization using the NCCL `AllReduce` collective. Given a named grid axis  $X$ , the operation  $\text{AllReduce}_X$  aggregates partial results by summation across that axis and replicates the accumulated result to all devices along the same axis.

#### 3.2.1 Communication Operators

We formalize the communication pattern by defining the operator  $\text{AllReduce}_X$  acting on a distributed tensor  $T$ , where  $T_{[i,j]}$  denotes the local block stored on the device at grid coordinate  $(i, j)$ . Depending on the aggregation axis, we define three variants:

$$\text{AllReduce}_R(T_{[i,j]}) = \sum_{k=1}^{|R|} T_{[k,j]}, \quad \text{AllReduce}_C(T_{[i,j]}) = \sum_{k=1}^{|C|} T_{[i,k]}, \quad \text{AllReduce}_G(T_{[i,j]}) = \sum_{k=1}^{|R|} \sum_{l=1}^{|C|} T_{[k,l]}. \quad (10)$$

Here,  $\text{AllReduce}_R$  aggregates data across the row axis,  $\text{AllReduce}_C$  across the column axis, and  $\text{AllReduce}_G$  across the entire device grid. In our distributed PDHG implementation,  $\text{AllReduce}_R$  is used to aggregate partial products in the computation of  $A^\top y$ , while  $\text{AllReduce}_C$  is used to sum partial results in the computation of  $Ax$ .

**Implementation Details.** For GPU-resident tensors, we use NCCL’s `AllReduce`, which provides high-performance collective communication over NVLink and high-speed interconnects. For small scalar quantities handled on the host, we use MPI’s `AllReduce` on the CPU.

#### 3.2.2 Distributed Primal–Dual Updates

The primal variables  $x$  are partitioned along the column axis  $C$  into blocks  $\{x_{[j]}\}$ , while the dual variables  $y$  are partitioned along the row axis  $R$  into blocks  $\{y_{[i]}\}$ .

For the primal update, the gradient term  $A^\top y^k$  is computed via partial products  $A_{[i,j]}^\top y_{[i]}^k$ , followed by an `AllReduce` across the row axis (R):

$$[A^\top y^k]_{[j]} = \text{AllReduce}_R(A_{[i,j]}^\top y_{[i]}^k).$$

The primal block update is then given by

$$x_{[j]}^{k+1} = \text{proj}_{\mathcal{X}_{[j]}}(x_{[j]}^k - \tau(c_{[j]} - [A^\top y^k]_{[j]})).$$

For the dual update, let  $\bar{x} = 2x^{k+1} - x^k$ . The partial products  $A_{[i,j]}\bar{x}_{[j]}$  are aggregated via an `AllReduce` across the column axis (C):

$$z_{[i]} = \text{AllReduce}_C(A_{[i,j]}\bar{x}_{[j]}),$$

followed by the local dual update

$$y_{[i]}^{k+1} = y_{[i]}^k - \sigma z_{[i]} - \sigma \cdot \text{proj}_{-\mathcal{S}_{[i]}}(\sigma^{-1}y_{[i]}^k - z_{[i]}).$$

### 3.2.3 Distributed KKT Error Computation

Convergence is monitored by evaluating the KKT conditions, including primal feasibility, dual feasibility, and the primal–dual gap. Under the 2D device grid, residual vectors and objective terms are distributed and, in some cases, replicated across devices. Global KKT metrics are obtained by aggregating local contributions using collective communication, with appropriate normalization to account for replication along the row and column axes.

Specifically, the distributed KKT quantities are computed as

$$\begin{aligned} \|r_p\|^2 &= \text{AllReduce}_R(\| \text{AllReduce}_C(A_{[i,j]}x_{[j]}) - b_{[i]} \|^2) \\ \|r_d\|^2 &= \text{AllReduce}_C(\| c_{[j]} - \text{AllReduce}_R(A_{[i,j]}^\top y_{[i]}) \|^2) \\ \text{Obj}_P &= \text{AllReduce}_C(c_{[j]}^\top x_{[j]}) \\ \text{Obj}_D &= -\text{AllReduce}_R(p(-y_{[i]}; (\ell_c)_{[i]}, (u_c)_{[i]})) + \text{AllReduce}_C(s_{[j]}^\top x_{[j]}) \\ \text{Gap} &= |\text{Obj}_P - \text{Obj}_D|, \end{aligned}$$

where  $s_{[j]} = (\text{proj}_{\mathcal{X}_j}(x_j - \tau g_{[j]}) - (x - \tau g_j))/\tau$ ,  $g_j = c_{[j]} - \text{AllReduce}_R(A_{[i,j]}^\top y_{[i]})$ . Details of the distributed operations used in algorithmic enhancements are provided in Appendix A.4.

## 3.3 Partition Strategy

Achieving high parallel efficiency in distributed sparse optimization requires addressing two key challenges: irregular sparsity patterns that cause computational load imbalance, and topology mismatches that increase communication overhead. We address these by introducing the following strategies.

### 3.3.1 Adaptive Grid Topology Selection

In the two-dimensional grid partitioning scheme, communication overhead is dominated by `AllReduce` operations along the row and column axes. To reduce both latency and bandwidth costs, the aspect ratio of the processor grid  $\mathcal{G} = |R| \times |C|$  should match the aspect ratio of the constraint matrix  $A \in \mathbb{R}^{m \times n}$ .

Specifically, the communication volume in the primal update  $A^\top y$  scales with the local column size  $n/|C|$ , while that of the dual update  $Ax$  scales with the local row size  $m/|R|$ . Although NNZ-based partitioning may lead to irregular local shapes, the random shuffling strategy yields approximately uniform partitions, allowing us to use these estimates for topology selection. When  $m \gg n$ , dual updates dominate communication, and choosing a grid with  $|R| > |C|$  reduces the local data volume and balances communication across axes.

Given a fixed number of processes  $N_{\text{procs}}$ , we select grid dimensions  $(|R|, |C|)$  by enumerating factor pairs with  $|R| \times |C| \leq N_{\text{procs}}$  and choosing the pair whose aspect ratio  $|R|/|C|$  best matches  $m/n$ . This adaptive strategy aligns the communication topology with the problem structure.

### 3.3.2 Random Permutation

Irregular sparsity patterns can lead to severe load imbalance under a static two-dimensional partition. A natural remedy is to randomly permute rows and columns before partitioning. However, a fully random permutation, while effective at balancing nonzeros, introduces new inefficiencies.

**Issues of Fully Random Permutation** Real-world LP instances often exhibit structured sparsity, such as clustered nonzeros, staircase patterns, or block-diagonal structure. Under a naive 2D partition, these structures can result in highly uneven nonzero distributions across devices. Although a full random permutation of all rows and columns equalizes the nonzero counts statistically, it destroys local sparsity structure and fragments dense sub-blocks. This leads to poor memory locality and uncoalesced access patterns, substantially degrading GPU SpMV performance.

**Block-wise Random Permutation.** To balance global load distribution with local memory efficiency, we adopt a block-wise random permutation strategy. We partition rows and columns into contiguous blocks of size  $B$  (e.g.,  $B = 64$

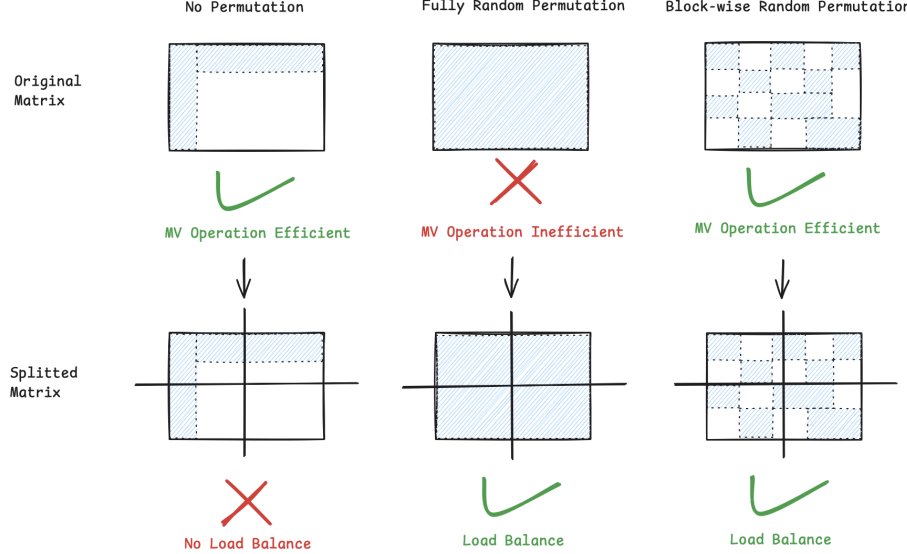


Figure 2: Comparison of matrix permutation strategies for distributed sparse optimization. **Left:** Natural ordering preserves local dense structures and favors memory coalescing, but causes severe load imbalance across devices. **Middle:** Full random permutation achieves uniform load distribution but destroys local sparsity, leading to irregular memory access and degraded SpMV performance. **Right:** Block-wise random permutation balances load while preserving dense micro-structures, enabling scalable and efficient GPU execution under 2D partitioning.

or 128) and apply random permutations over these blocks rather than individual indices. This approach disperses dense regions evenly across the  $|R| \times |C|$  device grid while preserving dense micro-structures within each  $B \times B$  block, enabling efficient, vectorized SpMV on GPUs.

### 3.3.3 NNZ-based Partitioning

After permutation, we partition the matrix using a heuristic based on cumulative nonzero counts (NNZ), applied independently along each grid axis.

For a grid axis  $X \in R, C$  of size  $|X|$ , let  $\text{nnz}_k$  denote the number of nonzeros in the  $k$ -th row (for  $X = R$ ) or the  $k$ -th column (for  $X = C$ ). We select partition boundaries  $\{p_0, p_1, \dots, p_{|X|}\}$  such that

$$\sum_{k=p_i}^{p_{i+1}-1} \text{nnz}_k \approx \frac{\text{nnz}(\tilde{A})}{|X|}.$$

This balances the workload along the one-dimensional projections of the matrix. Although this procedure does not enforce equal NNZ counts for every individual 2D block, in practice, the combination of random shuffling and axis-wise balancing yields a sufficiently uniform distribution for efficient parallel execution.

### 3.4 Device Communication Analysis

In the distributed PDHG implementation, inter-device communication is the primary bottleneck for scalability. We analyze the communication costs of each algorithmic component under a two-dimensional processor grid with axes  $R$  and  $C$ , which partitions the constraint matrix  $A$  into local blocks  $A_{[i,j]}$ .

The core PDHG loop—consisting of primal and dual updates together with the Halpern extrapolation—dominates the runtime. As shown in Section 3.2, each inner iteration requires synchronizing partial matrix–vector products via two vector AllReduce operations. Specifically, the dual update aggregates partial gradients  $A_{[i,j]}^\top y_{[i]}$  across the row axis  $R$ , incurring a communication volume of  $\mathcal{O}(n/|C|)$ . Similarly, the primal update aggregates partial constraint violations  $A_{[i,j]} x_{[j]}$  across the column axis  $C$ , with communication volume  $\mathcal{O}(m/|R|)$ . In contrast, the Halpern extrapolation is purely element-wise and requires no communication.

Every  $K$  iterations, the algorithm evaluates KKT residuals and canonical norms for convergence monitoring and restart decisions. This evaluation requires exact matrix–vector products, rather than intermediate quantities from the main loop, and thus involves three distributed products:  $Ax^k$ ,  $A^\top y^k$ , and  $A(x^k - x^0)$ . Consequently, this phase incurs three

additional vector AllReduce operations, followed by inexpensive global scalar reductions to compute norms and duality gaps. Owing to the high cost of vector synchronization, this evaluation is performed infrequently to reduce overhead.

Table 1 summarizes the communication complexity of the distributed PDHG algorithm.

Table 1: Communication Analysis per Operation

Operation	Comm. Type	Axis	Data Size	Frequency
<b>Main Loop</b>				
Primal Step ( $A^\top y$ )	Vector Sum	$R$	$\mathcal{O}(n/ C )$	1 per iter
Dual Step ( $Ax$ )	Vector Sum	$C$	$\mathcal{O}(m/ R )$	1 per iter
Halpern Update	None	-	0	-
<b>KKT Evaluation</b>				
Matrix Products	Vector Sum	$R, C$	$\mathcal{O}(n/ C  + m/ R )$	$1/K$ iters
Residual Norms	Scalar Sum	$G$	$\mathcal{O}(1)$	$1/K$ iters
Gap Calculation	Scalar Sum	$G$	$\mathcal{O}(1)$	$1/K$ iters
<b>Restart Logic</b>				
Restart Check	Vector Sum	$R, C$	$\mathcal{O}(n/ C  + m/ R )$	$1/K$ iters
Apply Restart	None	-	0	-
Weight Update	Scalar Sum	$G$	$\mathcal{O}(1)$	On Restart

## 4 Numerical Experiments

All distributed experiments were conducted on a high-performance computing node equipped with eight NVIDIA H100 GPUs, each with 80 GB of HBM3 memory, interconnected via NVLink to enable high-bandwidth peer-to-peer communication. The host system features a dual-socket configuration with Intel Xeon Platinum 8462Y+ processors, providing 64 physical cores (32 per socket) and 128 hardware threads in total.

Our distributed solver is implemented entirely in the Julia programming language. GPU execution is handled via `CUDA.jl`, with custom kernels for element-wise operations and NVIDIA cuSPARSE for optimized sparse matrix–vector multiplication. Inter-device communication follows a hybrid design: `MPI.jl` is used for control flow and scalar reductions, while `NCCL.jl` provides high-performance collective communication (e.g., `AllReduce`) for the vector synchronizations required by the core PDHG iterations.

### 4.1 Benchmark Datasets

To rigorously evaluate the performance and scalability of our solver, we utilize two distinct categories of benchmark datasets, ranging from standard academic problems to massive industrial-scale instances. For the initial validation and strong scaling analysis, we employ the MIPLIB 2017[Gleixner et al., 2021] relaxation set, comprising 383 diverse mixed-integer programming instances solved as linear programs, alongside Mittelmann’s LP benchmark[Mittelmann and Spellucci, 2005], which contains 49 challenging public instances. To ensure a consistent evaluation of algorithmic efficiency, we restrict our focus within these collections to instances that are known to be both feasible and bounded. For these standard benchmarks, we set the termination tolerance to  $\epsilon = 10^{-4}$ .

Moving beyond standard benchmarks, we further probe the capabilities of the distributed architecture using a curated, huge-scale dataset. This collection includes the notoriously difficult `zib03` instance from Koch et al., as well as large-scale PageRank formulations[Nesterov, 2014] derived from random graphs[Applegate et al., 2021] and real-world network datasets (e.g., LiveJournal)[Leskovec and Krevl, 2014] with up to 10 million nodes. We also incorporate extremely large multicommodity flow(`mcf`) and synthetic design matching(`sdm`) instances sourced from the large-scale linear programming test set\*. Furthermore, the suite includes Quadratic Assignment Problem (QAP) relaxations based on Adams-Johnson linearization[Adams and Johnson, 1994] (such as `tai50b` and `lipa50b`) and Unit Commitment problems(`ds1`, `ds2`), providing a robust test bed for high-dimensional sparse optimization. For these huge-scale instances, we adopt a tighter target accuracy of  $\epsilon = 10^{-6}$ , with the exception of the `mcf` instances, which are solved to a tolerance of  $10^{-4}$ .

### 4.2 Impact of Permutation and Partition Strategies

In Table 2, we analyze the effects of the proposed permutation and partitioning heuristics. As the table shows, the choice of permutation strategy is crucial for performance stability. The No Permutation baseline is highly vulnerable to catastrophic load imbalance, as evidenced by extreme runtimes on structured instances such as `zib03` (over

\* Available at <https://github.com/ohinder/large-scale-LP-test-problems>

7000 seconds on 8 GPUs) and the largest overall SGM10 of 220.08 seconds. Applying a Full Random permutation substantially alleviates this issue by redistributing nonzeros, but it is not optimal: by destroying the inherent block-dense substructures common in real-world LPs, it degrades memory locality and reduces the efficiency of sparse matrix–vector multiplication.

In contrast, the proposed Block Random permutation achieves a better trade-off. It effectively disperses dense regions to balance the workload while preserving local block structures that enable high-throughput computation. This robustness is reflected in consistently lower runtimes compared to full random permutation (SGM10 of 79.51s versus 86.80s).

Second, NNZ-based partitioning plays a complementary and indispensable role. In the absence of permutation, it yields the largest improvement by correcting severe imbalances in the natural ordering, reducing SGM10 from 220.08s to 194.13s. More importantly, NNZ partitioning continues to provide measurable gains even when combined with block-wise random permutation, further improving SGM10 from 79.51s to 75.85s. Since block shuffling alone does not guarantee perfectly uniform nonzero distributions, NNZ-based partitioning serves as a fine-grained balancing mechanism.

Overall, the combination of block-wise random permutation and NNZ-based partitioning delivers the most robust and efficient performance across the benchmark suite. Accordingly, all subsequent experiments adopt this configuration.

Table 2: Impact of permutation and partitioning strategies on solving time (seconds). We compare three permutation schemes (No Permutation, Full Random, Block Random) combined with either uniform (No NNZ) or nonzero-balanced (Yes NNZ) partitioning. Best results are marked in **bold**, and second-best are underlined.

Instance	GPU	No Permutation		Full Random		Block Random	
		No NNZ	Yes NNZ	No NNZ	Yes NNZ	No NNZ	Yes NNZ
sdm_50k_500k_15_10	4	328.20	<u>107.12</u>	227.02	237.99	142.49	<b>92.33</b>
	8	527.91	<u>377.41</u>	<u>69.06</u>	91.09	78.19	<b>60.90</b>
zib04	4	80.80	80.95	93.07	92.54	<u>79.70</u>	<b>78.27</b>
	8	61.94	62.18	63.38	65.05	<u>60.24</u>	<b>58.61</b>
zib03	4	2926.91	2017.57	501.96	502.93	<b>336.53</b>	<u>338.26</u>
	8	7368.89	2012.84	300.60	291.65	<b>243.76</b>	<u>245.29</u>
ds1_lp	4	777.84	682.63	157.49	155.88	<u>147.39</u>	<b>142.67</b>
	8	293.32	690.24	129.47	127.95	<u>124.65</u>	<b>122.27</b>
ds2_lp	4	3742.87	3299.29	748.69	746.62	<u>710.96</u>	<b>690.54</b>
	8	1407.81	3325.82	621.12	617.57	<u>594.08</u>	<b>591.10</b>
lipa50a	4	33.48	30.95	20.84	20.60	<u>19.95</u>	<b>19.95</b>
	8	35.48	33.18	17.08	<b>16.77</b>	<u>16.80</u>	16.94
lipa50b	4	35.03	32.12	21.82	21.32	<b>21.06</b>	<u>21.24</u>
	8	36.26	35.29	17.50	17.52	<b>17.26</b>	<u>17.31</u>
tai50a	4	34.96	32.08	21.98	21.65	<u>21.11</u>	<b>20.80</b>
	8	36.95	34.97	<b>17.25</b>	<u>17.36</u>	17.86	17.77
tai50b	4	101.52	81.91	53.94	54.91	<u>52.47</u>	<b>52.42</b>
	8	92.80	88.73	44.29	<u>43.60</u>	43.72	<b>42.59</b>
<b>SGM10</b>		220.08	194.13	86.80	87.96	<u>79.51</u>	<b>75.85</b>

### 4.3 Distributed PDLP on Benchmark Datasets

Tables 3 and 4 demonstrate the scalability of our distributed, grid-partitioned solver. For the smallest problem instances, specifically the MIPLIB Small subset with fewer than one million nonzeros, the single-GPU baseline achieves the lowest wall-clock time (5.81s versus 6.80s on 8 GPUs). This behavior is expected: for small problems, GPU resources are underutilized, and the computational gains from parallelism do not offset the additional communication overhead introduced by distributed AllReduce operations.

This slight performance regression on trivial instances is acceptable, as the distributed PDLP framework is designed to target large- and huge-scale problems where single-device solvers become bottlenecked by memory and throughput. This design goal is confirmed by the strong scaling observed on larger instances. In the MIPLIB Large category, the distributed implementation reduces SGM10 from 115.68s on a single GPU to 66.97s on 8 GPUs, demonstrating substantial performance gains from multi-GPU execution.

Table 3: Performance statistics (Shifted Geometric Mean, shift=10) on Mittelmann and MIPLIB datasets. Best results are marked in **bold**, and second-best are underlined.

Dataset	Metric	Number of GPUs			
		1	2	4	8
Mittelmann	Solved (< 3600s)	<b>46</b>	<b>46</b>	<b>46</b>	<b>46</b>
	Time (s) [SGM10]	21.26	<u>19.00</u>	<b>18.58</b>	19.24
	Iter/s [SGM10]	3233	<u>3617</u>	<b>3800</b>	<u>3621</u>
MIPLIB Small (100K - 1M)	Solved (< 1500s)	265	<b>267</b>	<b>267</b>	<u>266</u>
	Time (s) [SGM10]	<u>5.81</u>	<b>5.77</b>	6.12	6.80
	Iter/s [SGM10]	<b>3453</b>	<u>3172</u>	3019	2740
MIPLIB Medium (1M - 10M)	Solved (< 1500s)	<b>92</b>	<b>92</b>	<b>92</b>	<b>92</b>
	Time (s) [SGM10]	7.32	<b>6.68</b>	<u>6.70</u>	7.11
	Iter/s [SGM10]	3101	<b>3169</b>	<u>3161</u>	2965
MIPLIB Large (> 10M)	Solved (< 1500s)	13	<u>14</u>	<b>16</b>	<b>16</b>
	Time (s) [SGM10]	115.68	76.09	<u>69.06</u>	<b>66.97</b>
	Iter/s [SGM10]	1303	2049	<u>2564</u>	<b>2758</b>

The advantage becomes decisive on the huge-scale instances in Table 4, where computationally intensive problems like `sdm_50k_500k_15_10` and `zib03` achieve speedups of approximately  $6\times$  and  $3.3\times$  respectively on 8 GPUs. Most notably, our method obtains nearly linear acceleration on computationally intensive instances such as `mcf_2500_100_500`, achieving speedups of approximately  $3.1\times$  on 4 GPUs and  $6\times$  on 8 GPUs. Similarly, for the `sdm_50k_500k_15_10` instance, the solver attains a  $4.1\times$  speedup on 4 GPUs and  $6.2\times$  on 8 GPUs. These results demonstrate that the grid-partitioned architecture effectively translates additional compute resources into proportional reductions in solving time. This confirms that our distributed PDLP can harness the benefits brought by introducing more GPUs.

Table 4: Performance comparison: Single GPU vs. Distributed PDLP. Values represent wall-clock time in seconds. Best results are marked in **bold**, and second-best are underlined.

Source	Instance	m	n	nnz	Number of GPUs		
					1	4	8
Koch	zib03	19,731,970	29,128,799	104,422,573	812	<u>336</u>	<b>245</b>
Pagerank	rand 10m nodes	10,000,001	10,000,000	79,999,982	10	<u>5</u>	<b>4</b>
	com-livejournal	3,997,963	3,997,962	77,358,302	3	<u>2</u>	<b>1</b>
	soc-livejournal1	4,847,572	4,847,571	78,170,533	2	<u>1</u>	<b>1</b>
multicommodity-flow	mcf_2500_100_500	1,512,600	126,250,100	253,750,100	2943	<u>935</u>	<b>504</b>
	mcf_5000_50_500	2,775,050	126,250,050	253,750,050	9114	<u>2994</u>	<b>1677</b>
	mcf_5000_100_250	1,775,100	127,500,100	257,500,100	9173	<u>3159</u>	<b>1732</b>
design-matching	sdm_50k_500k_15_10	5,500,135	10,000,000	690,000,000	377	<u>92</u>	<b>61</b>
QAP	wil50				43	<u>31</u>	<b>25</b>
	lipa50a				27	<u>20</u>	<b>17</b>
	lipa50b	3,437,600	6,252,500	19,125,000	28	<u>21</u>	<b>17</b>
	tai50a				30	<u>21</u>	<b>18</b>
	tai50b				82	<u>52</u>	<b>43</b>
Unit Com.	ds1	641,037	659,145	21,577,566	279	<u>143</u>	<b>122</b>
	ds2				1288	<u>691</u>	<b>591</b>

## 5 Conclusion and Future Work

We presented a distributed implementation of the Primal-Dual Hybrid Gradient (PDHG) algorithm that leverages a two-dimensional grid partitioning strategy and block-wise random permutation to solve massive-scale linear programming problems on multi-GPU architectures. Our extensive experiments confirm that this framework overcomes single-node memory bottlenecks and achieves significant scalability on industrial-scale instances, delivering nearly linear speedups while maintaining full FP64 accuracy. Looking forward, we aim to further enhance performance by developing better permutation algorithms that jointly improve SpMV efficiency and load balancing and extending the distributed framework to support extensive problem types, such as quadratic and semi-definite programming.

## References

Warren P Adams and Terri A Johnson. Improved linear programming-based lower bounds for the quadratic assignment problem. *DIMACS series in discrete mathematics and theoretical computer science*, 16:43–77, 1994.

Alekh Agarwal, Alina Beygelzimer, Miroslav Dudík, John Langford, and Hanna Wallach. A reductions approach to fair classification. In *International conference on machine learning*, pages 60–69. PMLR, 2018.

Jacob M Aguirre, Diego Cifuentes, Vincent Guigues, Renato DC Monteiro, Victor Hugo Nascimento, and Arnesh Sudan. cuhallar: A gpu accelerated low-rank augmented lagrangian method for large-scale semidefinite programming. *arXiv preprint arXiv:2505.13719*, 2025.

David Applegate, Mateo Díaz, Oliver Hinder, Haihao Lu, Miles Lubin, Brendan O’Donoghue, and Warren Schudy. Practical large-scale linear programming using primal-dual hybrid gradient. *Advances in Neural Information Processing Systems*, 34:20243–20257, 2021.

Mosek ApS. Mosek optimization toolbox for matlab. *User’s Guide and Reference Manual, Version*, 4(1), 2019.

Jacob Austin, Sholto Douglas, Roy Frostig, Anselm Levskaya, Charlie Chen, Sharad Vikram, Federico Lebron, Peter Choy, Vinay Ramasesh, Albert Webson, and Reiner Pope. How to scale your model. 2025. Retrieved from <https://jax-ml.github.io/scaling-book/>.

Aharon Ben-Tal, Dick Den Hertog, Anja De Waegenaere, Bertrand Melenberg, and Gijs Rennen. Robust solutions of optimization problems affected by uncertain probabilities. *Management Science*, 59(2):341–357, 2013.

Kaihuang Chen, Defeng Sun, Yancheng Yuan, Guojun Zhang, and Xinyuan Zhao. Hpr-qp: A dual halpern peaceman-rachford method for solving large-scale convex composite quadratic programming. *arXiv preprint arXiv:2507.02470*, 2025.

Qi Deng, Qing Feng, Wenzhi Gao, Dongdong Ge, Bo Jiang, Yuntian Jiang, Jingsong Liu, Tianhao Liu, Chenyu Xue, Yinyu Ye, et al. New developments of ADMM-based interior point methods for linear programming and conic programming. *arXiv preprint arXiv:2209.01793*, 2022.

Lijun Ding, Haihao Lu, and Jinwen Yang. New understandings and computation on augmented lagrangian methods for low-rank semidefinite programming. *arXiv preprint arXiv:2505.15775*, 2025.

Edmund Eisenberg and David Gale. Consensus of subjective probabilities: The pari-mutuel method. *The Annals of Mathematical Statistics*, 30(1):165–168, 1959.

Guillermo Gallego and Garrett Van Ryzin. A multiproduct dynamic pricing problem and its applications to network yield management. *Operations research*, 45(1):24–41, 1997.

Harsha Gangammanavar and Suvrajeet Sen. Stochastic dynamic linear programming: A sequential sampling algorithm for multistage stochastic linear programming. *SIAM Journal on Optimization*, 31(3):2111–2140, 2021.

Dongdong Ge, Qi Huangfu, Zizhuo Wang, Jian Wu, and Yinyu Ye. Cardinal optimizer (copt) user guide. *arXiv preprint arXiv:2208.14314*, 2022.

Ambros Gleixner, Gregor Hendel, Gerald Gamrath, Tobias Achterberg, Michael Bastubbe, Timo Berthold, Philipp Christophel, Kati Jarck, Thorsten Koch, Jeff Linderoth, et al. Miplib 2017: data-driven compilation of the 6th mixed-integer programming library. *Mathematical Programming Computation*, 13(3):443–490, 2021.

LLC Gurobi Optimization. Gurobi optimizer reference manual. 2021.

Qiushi Han, Chenxi Li, Zhenwei Lin, Caihua Chen, Qi Deng, Dongdong Ge, Huikang Liu, and Yinyu Ye. A low-rank admm splitting approach for semidefinite programming. *arXiv preprint arXiv:2403.09133*, 2024a.

Qiushi Han, Zhenwei Lin, Hanwen Liu, Caihua Chen, Qi Deng, Dongdong Ge, and Yinyu Ye. Accelerating low-rank factorization-based semidefinite programming algorithms on gpu. *arXiv preprint arXiv:2407.15049*, 2024b.

Norio Hibiki. Multi-period stochastic optimization models for dynamic asset allocation. *Journal of Banking & Finance*, 30(2):365–390, 2006.

Yicheng Huang, Wanyu Zhang, Hongpei Li, Dongdong Ge, Huikang Liu, and Yinyu Ye. Restarted primal-dual hybrid conjugate gradient method for large-scale quadratic programming. [arXiv preprint arXiv:2405.16160](#), 2024.

Thorsten Joachims, Thomas Finley, and Chun-Nam John Yu. Cutting-plane training of structural svms. [Machine learning](#), 77(1):27–59, 2009.

Frank P Kelly, Aman K Maulloo, and David Kim Hong Tan. Rate control for communication networks: shadow prices, proportional fairness and stability. [Journal of the Operational Research society](#), 49(3):237–252, 1998.

Jure Leskovec and Andrej Krevl. Snap datasets: Stanford large network dataset collection, 2014.

Tianyi Lin, Shiqian Ma, Yinyu Ye, and Shuzhong Zhang. An ADMM-based interior-point method for large-scale linear programming. [Optimization Methods and Software](#), 36(2-3):389–424, 2021.

Zhenwei Lin, Zikai Xiong, Dongdong Ge, and Yinyu Ye. Pdcs: A primal-dual large-scale conic programming solver with gpu enhancements. [arXiv preprint arXiv:2505.00311](#), 2025.

Huikang Liu, Yicheng Huang, Hongpei Li, Dongdong Ge, and Yinyu Ye. Pdhcg: A scalable first-order method for large-scale competitive market equilibrium computation. [arXiv preprint arXiv:2506.06258](#), 2025.

Haihao Lu and Jinwen Yang. cupdlp.jl: A gpu implementation of restarted primal-dual hybrid gradient for linear programming in julia. [arXiv preprint arXiv:2311.12180](#), 2023a.

Haihao Lu and Jinwen Yang. A practical and optimal first-order method for large-scale convex quadratic programming. [arXiv preprint arXiv:2311.07710](#), 2023b.

Haihao Lu and Jinwen Yang. Pdot: A practical primal-dual algorithm and a gpu-based solver for optimal transport. [arXiv preprint arXiv:2407.19689](#), 2024a.

Haihao Lu and Jinwen Yang. Restarted halpern pdhg for linear programming. [arXiv preprint arXiv:2407.16144](#), 2024b.

Haihao Lu, Jinwen Yang, Haodong Hu, Qi Huangfu, Jinsong Liu, Tianhao Liu, Yinyu Ye, Chuwen Zhang, and Dongdong Ge. cupdlp-c: A strengthened implementation of cupdlp for linear programming by c language. [arXiv preprint arXiv:2312.14832](#), 2023.

Haihao Lu, Zedong Peng, and Jinwen Yang. cupdlpx: A further enhanced gpu-based first-order solver for linear programming. [arXiv preprint arXiv:2507.14051](#), 2025.

Hans D Mittelmann and P Spellucci. Decision tree for optimization software, 2005.

Yu Nesterov. Subgradient methods for huge-scale optimization problems. [Mathematical Programming](#), 146(1):275–297, 2014.

James B Orlin. Improved algorithms for computing fisher’s market clearing prices: Computing fisher’s market clearing prices. In [Proceedings of the forty-second ACM symposium on Theory of computing](#), pages 291–300, 2010.

Kalyan T Talluri and Garrett J Van Ryzin. [The theory and practice of revenue management](#), volume 68. Springer Science & Business Media, 2006.

Ben Taskar, Vassil Chatalbashev, Daphne Koller, and Carlos Guestrin. Learning structured prediction models: A large margin approach. In [Proceedings of the 22nd international conference on Machine learning](#), pages 896–903, 2005.

Gary R Waissi. [Network flows: Theory, algorithms, and applications](#), 1994.

Fangzhao Zhang and Stephen Boyd. Solving large multicommodity network flow problems on gpus. [arXiv preprint arXiv:2501.17996](#), 2025.

Guojun Zhang, Zhexuan Gu, Yancheng Yuan, and Defeng Sun. Hot: An efficient halpern accelerating algorithm for optimal transport problems. [IEEE Transactions on Pattern Analysis and Machine Intelligence](#), 2025.

## A Details of Algorithm Enhancement in cuPDLPx

The convergence of PDHG is analyzed using the canonical norm  $\|\cdot\|_P$ , where the metric matrix  $P$  is defined as:

$$P := P_{\eta, \omega} = \begin{bmatrix} \frac{\omega}{\eta} I & A^\top \\ A & \frac{1}{\eta\omega} I \end{bmatrix} \quad (11)$$

The iterate update is denoted as  $z^{k+1} = \text{PDHG}(z^k)$ , where  $z^k = [x^k; y^k]^\top$ .

### A.1 Reflected Halpern Iteration Scheme

Rather than using vanilla PDHG iterates, Lu and Yang [2024b] adopts the restarted Halpern PDHG (rHPDHG) scheme. This scheme interpolates between the standard PDHG iterate and an initial anchor point  $z^0$ :

$$z^{k+1} = \left( (1 + \gamma) \frac{k+1}{k+2} \text{PDHG}(z^k) - \gamma z^k \right) + \frac{1}{k+2} z^0 \quad (12)$$

This allows the algorithm to take more aggressive steps, resulting in stronger empirical performance Lu et al. [2025].

### A.2 Adaptive Restarting Strategy

The adaptive restart strategy is designed to ensure the anchor point remains relevant to the local geometry. A restart is triggered based on a fixed-point error metric  $r(z) = \|z - \text{PDHG}(z)\|_P$ . The criteria for triggering a restart include:

- **Sufficient Decay:**  $r(z^{n,k}) \leq \beta_{\text{sufficient}} r(z^{n,0})$ .
- **Necessary Decay:**  $r(z^{n,k}) \leq \beta_{\text{necessary}} r(z^{n,0})$  and  $r(z^{n,k}) > r(z^{n,k-1})$ .
- **Artificial Restart:**  $k \geq \beta_{\text{artificial}} T$ , where  $T$  is the total iterations.

### A.3 PID-Controlled Primal Weight Update

To balance progress between the primal and dual spaces, the primal weight  $\omega$  is dynamically adjusted using a Proportional-Integral-Derivative (PID) controller at each restart Lu and Yang [2024b]. Logarithmic error  $e^n$  is defined as the distance between the primal and dual to the anchor:

$$e^n = \log \left( \frac{\sqrt{\omega^n} \|x^{n,t} - x^{n,0}\|_2}{\frac{1}{\sqrt{\omega^n}} \|y^{n,t} - y^{n,0}\|_2} \right) \quad (13)$$

The weight for the next epoch is updated as:

$$\log \omega^{n+1} = \log \omega^n - \left[ K_P \cdot e^n + K_I \sum_{i=1}^n e^i + K_D (e^n - e^{n-1}) \right] \quad (14)$$

where  $K_P$ ,  $K_I$ , and  $K_D$  are the controller coefficients.

### A.4 Distributed Operators for Algorithm Enhancements

The advanced heuristics in cuPDLPx, namely the Reflected Halpern Iteration, Adaptive Restarting, and PID-controlled weight updates—require specific distributed operations to function correctly on the  $R \times C$  processor grid. We define these operations using the partition notation established in Section 3.2, where the primal vector  $x$  is partitioned along the column axis  $C$  into blocks  $x_{[j]}$ , and the dual vector  $y$  is partitioned along the row axis  $R$  into blocks  $y_{[i]}$ .

#### A.4.1 Distributed Halpern Update

The Halpern iteration scheme computes a linear combination of the current PDHG output, the previous iterate  $z^k$ , and the anchor point  $z^0$ . Since the anchor point  $z^0$  follows the identical partitioning scheme as the current iterate, this update is performed locally on each device without communication. Let  $z_{[i,j]}^k = (x_{[j]}^k, y_{[i]}^k)$  denote the local portion of the primal-dual pair stored on device  $(i, j)$ . The update is given by:

$$z_{[i,j]}^{k+1} = \left( (1 + \gamma) \frac{k+1}{k+2} \text{PDHG}(z_{[i,j]}^k) - \gamma z_{[i,j]}^k \right) + \frac{1}{k+2} z_{[i,j]}^0 \quad (15)$$

This locality property ensures that the acceleration step introduces zero communication overhead.

#### A.4.2 Distributed Fixed-Point Error

The restarting strategy relies on the fixed-point error metric  $r(z) = \|z - \text{PDHG}(z)\|_P$ . The computation of the squared norm  $\|\Delta z\|_P^2$  (where  $\Delta z = z - \text{PDHG}(z)$ ) involves a coupling term due to the off-diagonal blocks of the metric matrix  $P$ :

$$\|\Delta z\|_P^2 = \frac{\omega}{\eta} \|\Delta x\|^2 + \frac{1}{\eta\omega} \|\Delta y\|^2 + 2\langle A\Delta x, \Delta y \rangle \quad (16)$$

To compute this efficiently without reconstructing global vectors, we decompose the calculation into distributed scalar reductions:

- **Primal and Dual Norms:** The squared Euclidean norms are computed by summing the local squared norms across the respective partition axes and aggregating globally:

$$\|\Delta x\|^2 = \text{AllReduce}_G \left( \frac{1}{|R|} \sum \|\Delta x_{[j]}\|^2 \right) \quad (17)$$

$$\|\Delta y\|^2 = \text{AllReduce}_G \left( \frac{1}{|C|} \sum \|\Delta y_{[i]}\|^2 \right) \quad (18)$$

The factors  $1/|R|$  and  $1/|C|$  account for the replication of variables across the orthogonal grid axes.

- **Interaction Term ( $\langle A\Delta x, \Delta y \rangle$ ):** Directly computing  $A\Delta x$  would require an expensive vector `AllReduce`. Instead, we utilize the linearity of the inner product. Each device computes the local dot product between its partial matrix-vector result ( $A_{[i,j]}\Delta x_{[j]}$ ) and its local dual block ( $\Delta y_{[i]}$ ). We then aggregate these scalars globally:

$$\langle A\Delta x, \Delta y \rangle = \text{AllReduce}_G ((A_{[i,j]}\Delta x_{[j]})^\top \Delta y_{[i]}) \quad (19)$$

This approach reduces the communication volume from  $\mathcal{O}(m+n)$  (vector reduction) to  $\mathcal{O}(1)$  (scalar reduction).

#### A.4.3 Distributed PID Weight Update

The PID controller adjusts the primal weight  $\omega$  based on the logarithmic error  $e^n$ , which depends on the global distances to the anchor point:

$$d_x^2 = \|x^{n,t} - x^{n,0}\|_2^2, \quad d_y^2 = \|y^{n,t} - y^{n,0}\|_2^2 \quad (20)$$

These distances are computed using global scalar reductions analogous to the norm calculations above. Once the scalars  $d_x$  and  $d_y$  are synchronized via `AllReduceGlobal`, the PID update for  $\omega^{n+1}$  is performed redundantly on every device. This guarantees that the scalar parameter  $\omega$  remains consistent across the entire grid without requiring a separate broadcast step.